Int Nano Lett (2017) 7:257–265
https://doi.org/10.1007/s40089-017-0216-0

ORIGINAL ARTICLE

Tuned optical transmittance in single-step-derived silica aerogels through pH-controlled microstructure

Wesam A. A. Twej[1] · Ashraf M. Alattar[1] · Matthew Drexler[2] · Faisal M. Alamgir[2]

Received: 6 March 2017 / Accepted: 4 August 2017 / Published online: 1 September 2017

Abstract We have systematically studied the relationship between synthesis pH and morphological and optical properties of silica aerogels. We have determined through SEM and BET that there is a systematic correlation between the pH of the initial silica solution and the surface area, porosity, and pore size of the resulting aerogel. We find that optical transmittance, particularly its wavelength dependence (dispersion), is strongly governed by the microstructure and, therefore, synthesis pH. We have determined that the microstructure of the aerogels fall into three broad categories: monostructural, which is characterized by repeating elongated microstructural features; fractal, which shows a distinctive structure that is emulated on multiple length scales; and isotropic, which is characterized by having no distinct features in its microstructure. Simply by controlling the pH of the synthesis environment, we can tune the optical properties of silica aerogels through pH controlled the microstructural modification. We have found that pH = 1–5 gives high dispersion, pH = 6–7 results in low transmittance and low dispersion, pH = 8 shows the highest transmittance with the lowest dispersion, and pH = 9–10 transitions back to lower transmittance and higher dispersion.

Keywords Transmittance · Aerogel · pH value · Structural properties · Optical properties

✉ Wesam A. A. Twej
Wesam961@yahoo.co.in

Ashraf M. Alattar
ashraf_alattar2000@yahoo.com

Matthew Drexler
mdrexler3@gatech.edu

Faisal M. Alamgir
faisal.alamgir@mse.gatech.ed

[1] Physics Department, University of Baghdad, Baghdad, Iraq

[2] School of Material Science and Engineering, Georgia Institute of Technology, Atlanta, GA 3003, USA

Introduction

Aerogels have been studied for more than 80 years, the first samples having been synthesized by Kistler [1]. Since the 1980s, researchers have extensively studied their fractal structures and mechanisms of formation in sol–gel processes, such as noteworthy works by Schaefer and Keefer [2, 3]. Problems concerning the self-organization of these systems have also been thoroughly reviewed in surveys by Roldugin [4, 5].

Aerogels can be produced via sol–gel processes. Linear structures are formed during the final sol aging stage, which then transform into nanoglobules, the density of which depends on the pH of the solution. These nanoglobules form homogeneously throughout the sol and then aggregate to form structures during the final stages of growth whose size is determined by diffusion-limited aggregation [6]. Gelation is followed by the drying of the wet gel in an autoclave under supercritical conditions for CO_2, a process that leads to a pure, homogeneous product with low density, high specific surface area, and high porosity [7, 8]. This potentially allows them to be used in numerous applications, such as catalysis, fuel storage tanks, low dielectric constant materials, and fine particle collection [9, 10].

Because the kinetics of network formation govern its final structure, the gelation pH as well as the type and concentration of ions present in solution are known to

affect the final properties of the aerogel [11, 12]. Iler divides the silica polymerization process into three pH domains, pH <2, pH 2–7, and pH >7 [13], and others have contributed significant advances to our understanding of the mechanism of gel formation over these pH ranges [14–16]. Control of pH can, therefore, influence microstructure at the length scale of the visible spectrum, which in turn affects the magnitude of optical transmittance and its wavelength dependence (dispersion).

Silica aerogels are materials well suited for high power nonlinear optical applications. Gentilini et al. [17] showed that the structural disorder due to the porous solid-state gel has a significant effect onto the generation of optical shock waves. The optical transparency of silica aerogel is tied closely to scattering centres within its microstructure [18]. This transparency, particularly in the solar spectrum, is crucial for many solar related applications [19–22].

There appears, however, to be a dearth of studies in the literature which cover a direct relationship between solution pH and the subsequent optical properties of aerogels. In this paper, we try to carefully explore these relations and further examine whether a single synthesis parameter, the pH, can be used to tune the transmittance and dispersion properties of silica aerogels.

Experimental

Materials

Tetraethylorthosilicate (TEOS >99.0% purity), spectroscopic grade ethyl alcohol (200 proof, >99.5% purity), and ammonium fluoride (>98.0% purity) were obtained from Sigma Aldrich. Hydrochloric acid (0.15 M, >99.0% purity) was supplied by Amresco, and ammonium hydroxide was supplied by BDH.

Synthesis

Silica gels were prepared via the following single-step process. TEOS, ethanol, water, and a solution used to modify pH were mixed using a volume ratio of 2.5:10:2:*X*, where *X* was varied to achieve the desired pH. Hydrochloric acid was used to reduce pH while an ammonium fluoride–ammonium hydroxide solution, prepared by adding 0.463 g of ammonium fluoride and 5.695 ml of ammonium hydroxide to 25 ml of water, was used to raise pH. The solutions were stirred at 30 °C for 1 h under magnetic stirring. The resulting sol was allowed to gel in 3.1 cm diameter plastic tubes and then aged in the same tubes for 22 h at room temperature. To remove any unreacted monomer from the gel network, the gels were washed with pure ethanol every 24 h five times. The gels were then dried in an autoclave. The gels were submerged in ethanol to prevent drying too quickly, CO_2 was used to maintain the pressure between 50 and 60 bar, and ice was used to maintain the temperature at 0 °C. Ethanol would be flushed from the system twice a day by depressurizing to 45 bar, then the pressure would be brought back to between 50 and 60 bar. This process would be repeated for anywhere between 1 and 5 days depending on the size of the sample. Once the ethanol was completely removed from the system, the temperature and pressure were raised to above 32 °C and 73 bar and held at that temperature and pressure 3 h. The autoclave was then depressurized over 5–6 h at a constant temperature of 32 °C. The sizes of the resulting aerogel samples were about 28–30 mm in diameter and 13 mm in thickness.

Characterization

We measured optical transparency using an Ultrospec. 4300 pro UV–Vis Spectrophotometer at 1 nm intervals over the range from 400 to 700 nm to construct optical transmittance curves. To calculate average transmittance, we integrated the area under each curve and divided by the range (300 nm). We observed the morphology and microstructure of silica aerogel samples with scanning electron microscopy (SEM), using the secondary electron detector of a Zeiss Ultra 60 FE-SEM. We measured the average pore size and specific surface area of the aerogel samples using the BET method with a Micromeritics ASAP 2020, employing nitrogen adsorption–desorption. Finally, we determined the apparent densities of the samples by weighing cylindrical samples of known dimensions.

Results

UV–Vis

Figure 1 presents transmittance as a function of wavelength for samples prepared at pH values ranging from 1 to 10.

Interestingly, the pH = 5, 6, 7, and 10 samples maintain a relatively low transmittance over the entire visible spectrum, whereas the transmittance of the pH = 1, 2, 3, 4, 8, and 9 samples increase with increasing wavelength.

Figure 2 depicts the average transmittance of silica aerogels prepared with different pH values along with pictures of each sample to show their transparency. The sample prepared using pH = 8 had the highest transmittance.

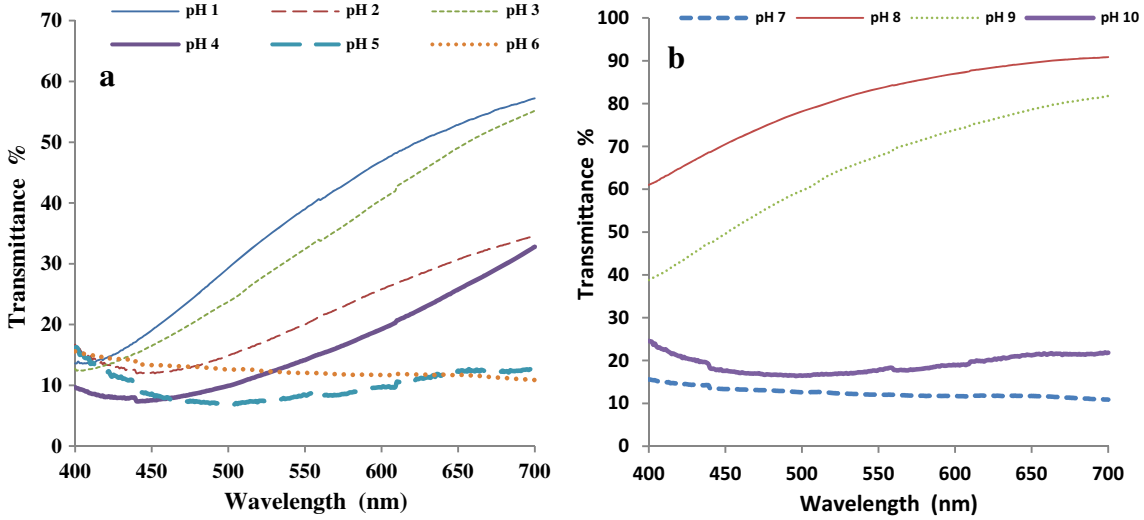

Fig. 1 Transmittance spectra (percent transmitted) of aerogel samples at **a** low and **b** high pH values

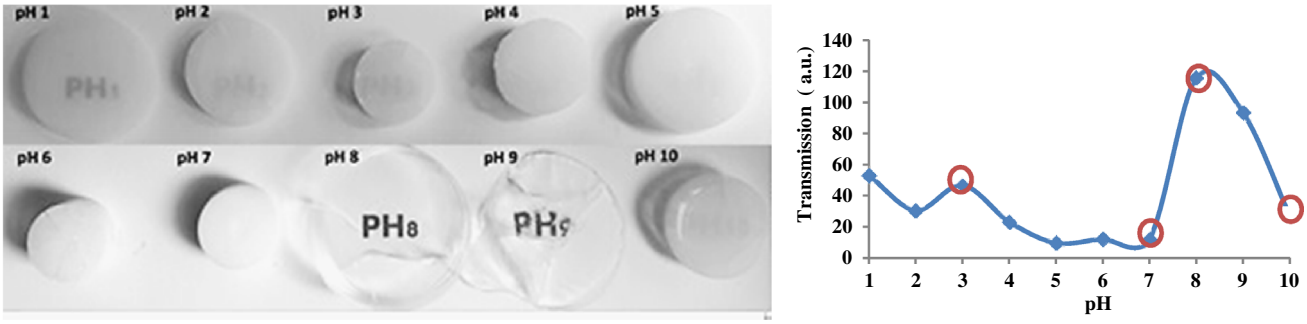

Fig. 2 Effect of the final preparation pH value on transmittance (*left*) and the average transmittance value in the entire visible region as a function of pH (*right*). The *red circles* are samples chosen to represent intermediate (pH = 3), low (pH = 7 and 10), and high (pH = 8) transmittance for which SEM images are given in Fig. 6

Surface area and pore size measurements

We found pore volumes using a single condensation point (relative pressure = 0.99), and surface area using five points in the linear region at a relative pressure between 0.05 and 0.35. The results of these tests did not deviate from one another more than the expected error of the test (± 5%) when taken multiple times on the same sample.

Figure 3 shows the linear isotherm plots for each aerogel sample. The plots fall into two categories according to their adsorption behavior [23]. The plots in the first category, shown in Fig. 3a, have a relatively linear absorption with relative pressure in comparison with those in the second category, where more than half of their adsorption occurs at a relative pressure greater than 0.9.

Figure 4 summarizes the influence of preparation pH on surface area, pore size, and pore volume. In general, the surface area of silica aerogels decreases as preparation pH increases, as shown in the dashed curve in Fig. 4a. Figure 4b demonstrates the variation of pore volume and size with preparation pH, and it appears that pore volume and size exhibit a similar behaviour with respect to pH. Each has a global maximum at pH = 8 and another local maximum below pH = 7; this occurs at pH = 2 for pore volume and pH = 4 for pore size. It is notable that the preparation of aerogel under neutral conditions yields the lowest pore size, pore volume, and surface area.

Figure 5 shows the pH dependence of surface area calculated from two other methods, a t-plot and the Langmuir isotherm. It is clear from Fig. 5a that aerogel prepared under pH = 7 still has the lowest surface area, even when using different models to calculate it. The t-plot method also finds that there is a minimum in the pore volume and size at pH = 8 and that there is a general decrease in pore volume and size as pH increases.

Table 1 summarizes the N2 adsorption–desorption isotherms measurements at 77 K for silica aerogels prepared under pH = 1–10.

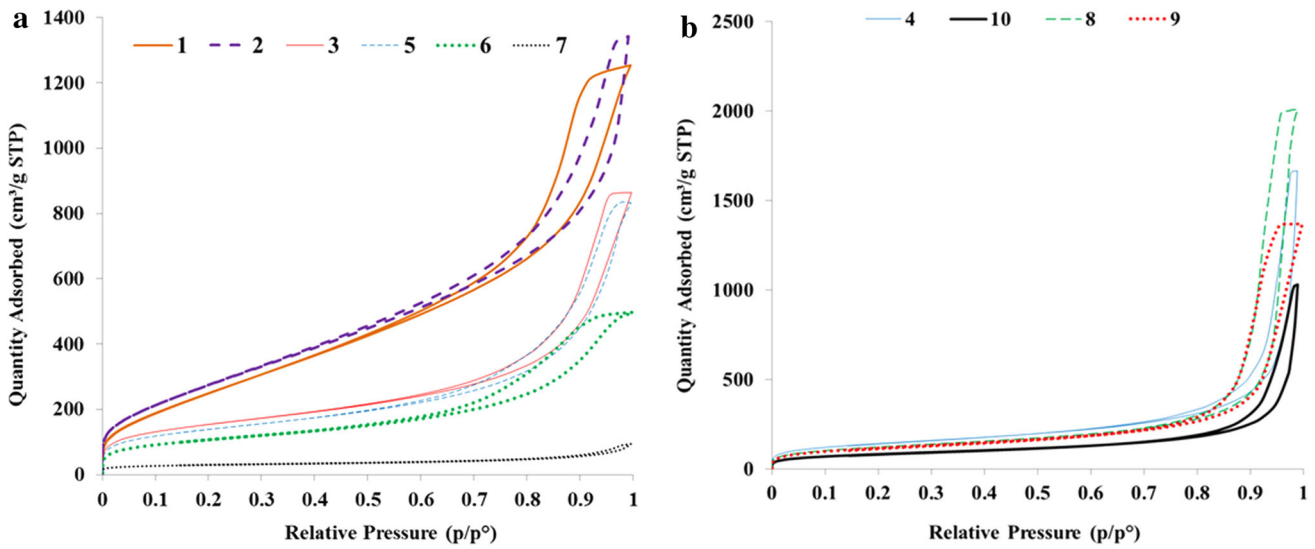

Fig. 3 Nitrogen adsorption/desorption isotherms (IUPAC) at 77.35 K for aerogels prepared at the final pH values **a** = 1, 2, 3, 5, 6, and 7 and **b** = 4, 8, 9, and 10

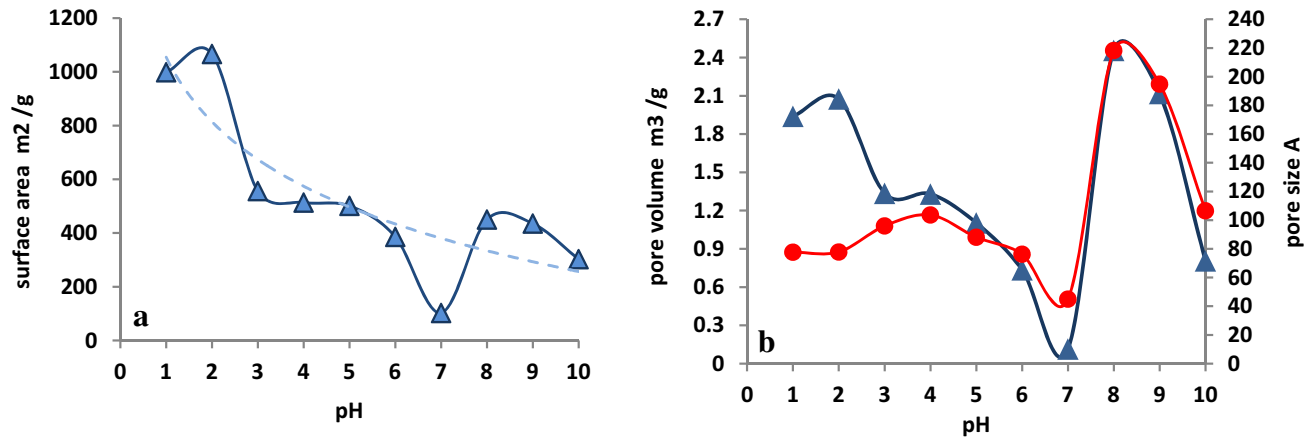

Fig. 4 Influence pH on **a** specific surface area and **b** single-point adsorption total pore volume of pores in the synthesized aerogels

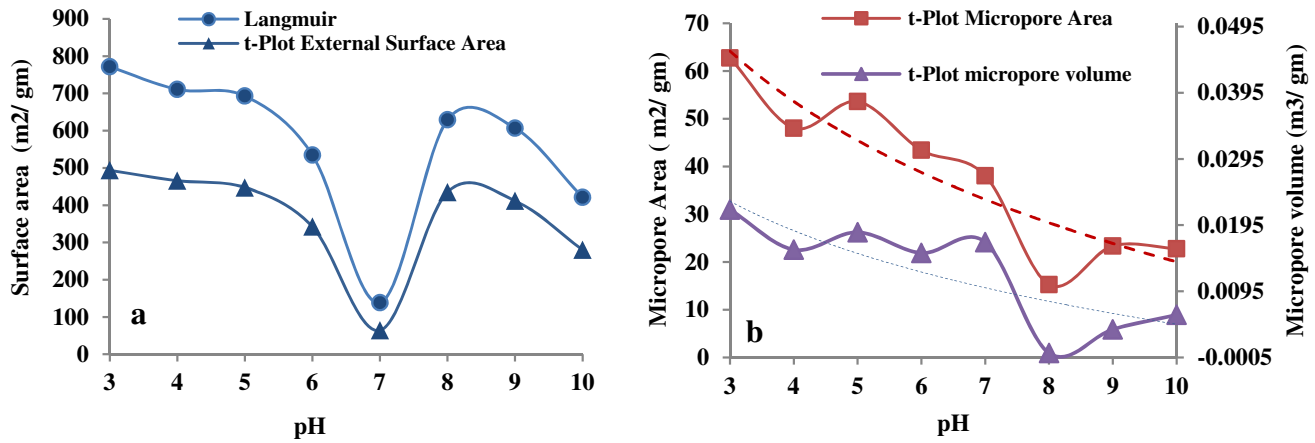

Fig. 5 Influence of pH on **a** surface area and **b** pore volume and size

Table 1 Nitrogen sorption measurement for silica aerogel

pH	Surface area (m^2/gm)				Pore volume (cm^3/gm)			Pore size (A°)			Porosity%	Measured density (gm/cm^3)
	Single	BET	BJH Ads	BJH Des	Single	BJH Ads	BJH Des	BET	BJH Ads	BJH Des		
1	934.18	998.25	1011.09	1105.61	1.93	1.79	1.82	77.71	71.01	65.93	97.5	0.05049
2	1009.3	1066.4	987.78	1084.19	2.07	1.89	1.93	77.83	76.52	71.41	97.3	0.05593
3	535.09	556.34	502.35	540.68	1.33	1.33	1.36	96.02	106.25	100.77	97.2	0.05779
4	493.88	513.73	482.88	514.91	1.33	2.6	2.59	103.6	215.45	201.24	97	0.06317
5	481.87	500.98	477.34	507.36	1.1	1.31	1.3	88.1	110.16	103.04	96.4	0.07504
6	371.39	385.75	367.54	398.15	0.73	0.79	0.78	76.3	86.27	78.95	96.2	0.07731
7	101.24	102.19	53.72	54.01	0.11	0.12	0.12	44.91	92.44	91.61	93.9	0.12976
8	428.58	450.26	460.49	552.32	2.45	3.11	3.12	218.28	270.72	225.22	97.7	0.04730
9	413.86	435.01	436.35	485.51	2.12	2.13	2.12	194.88	195.37	175.06	97.6	0.05232
10	289.2	302.85	286.48	303.21	0.8	1.60	1.6	106.59	224.56	211.34	97.2	0.05935

Morphology

Figure 6 shows images of the aerogel microstructure obtained from SEM. It is clear from these images that the reaction pH value has a significant effect on aerogel morphology [2, 3].

The images of the pH = 1 as well as pH = 3 aerogels show parallel ridges that rise out of the fracture surface, while the pH = 2 sample is composed of branched clusters of smaller particles. The pH = 4 aerogel appears to be a combination of the two, having branched clusters that form into ridges. The pH = 5 and 6 samples have the same structure as pH = 2, but the particles in pH = 5 are larger and have fused together in pH = 6. pH = 7 has a continuous and highly cross-linked network, and this, coupled with its smaller pores size, leads to a very open structure, where individual particles cannot be distinguished. Above this pH, the micro- and nanostructural features seen in the lower pH samples begin to return, with the ridged structure of the fracture surface beginning to emerge in the pH = 8 sample. These ridges become more prominent in the pH = 9 sample, and the nanoparticles begin to form branched clusters just as in the pH = 2 sample.

We classify the various different microstructures shown in Fig. 6 into three broad categories, monostructural (M1), fractal (M2), and isotropic (M3), and have found that they are linked to the aerogel's optical properties. Figure 7 shows for SEM images of four samples chosen for their transmittance (Fig. 2), and each exhibits a distinct microstructure that falls into one of these three categories. The pH = 3 sample gives an example of the monostructural microstructure. The fracture surface appears to be composed of elongated ridges, each ridge being composed of serrations less than a micrometre in size, as the red outlines in the figure indicate. The pH = 7 and pH = 10 samples have a very similar microstructure that appears to be fractal in nature as indicated by the red outline. The pH 8 sample has a much finer pore size than other samples, its pores being nearly imperceptible at the same magnification much like the pH = 3 sample, but unlike the pH = 3 sample, the facture surface gives no indication of any directionality to its features, making it isotropic.

Discussion

Highly transparent aerogels are normally prepared using a two-step method [24, 25]. In this work, silica aerogels were prepared using a single step method to reduce the number of synthesis factors and, therefore, better establish the influence of pH on microstructure and optical properties.

Since the solubility of silica is quite low below pH = 2, ripening after nanoparticle formation is restricted to less than 2 nm in diameter, causing gel networks to form by aggregation rather than particle growth [13]. It is generally agreed that between pH = 2 and pH = 6, condensation preferentially occurs on larger particles. This leads to a larger average particle size and causes crosslinking between particles to occur only after the depletion of the monomer [15]. At pH values greater than 7, condensed species are ionized and, therefore, mutually repulsive. Growth occurs primarily through the addition of monomers to the more highly condensed particles rather than by particle aggregation [16]. It has been claimed that, in general, the sol–gel-derived silicon oxide networks under acid-catalysed conditions yield primarily linear or randomly branched polymers, while base-catalysed conditions yield more highly branched clusters which do not interpenetrate prior to gelation and thus behave as discrete clusters [13]. These differences in gel formation explain how silica aerogels synthesized under different conditions would possess different microstructures, as shown in Figs. 6 and 7.

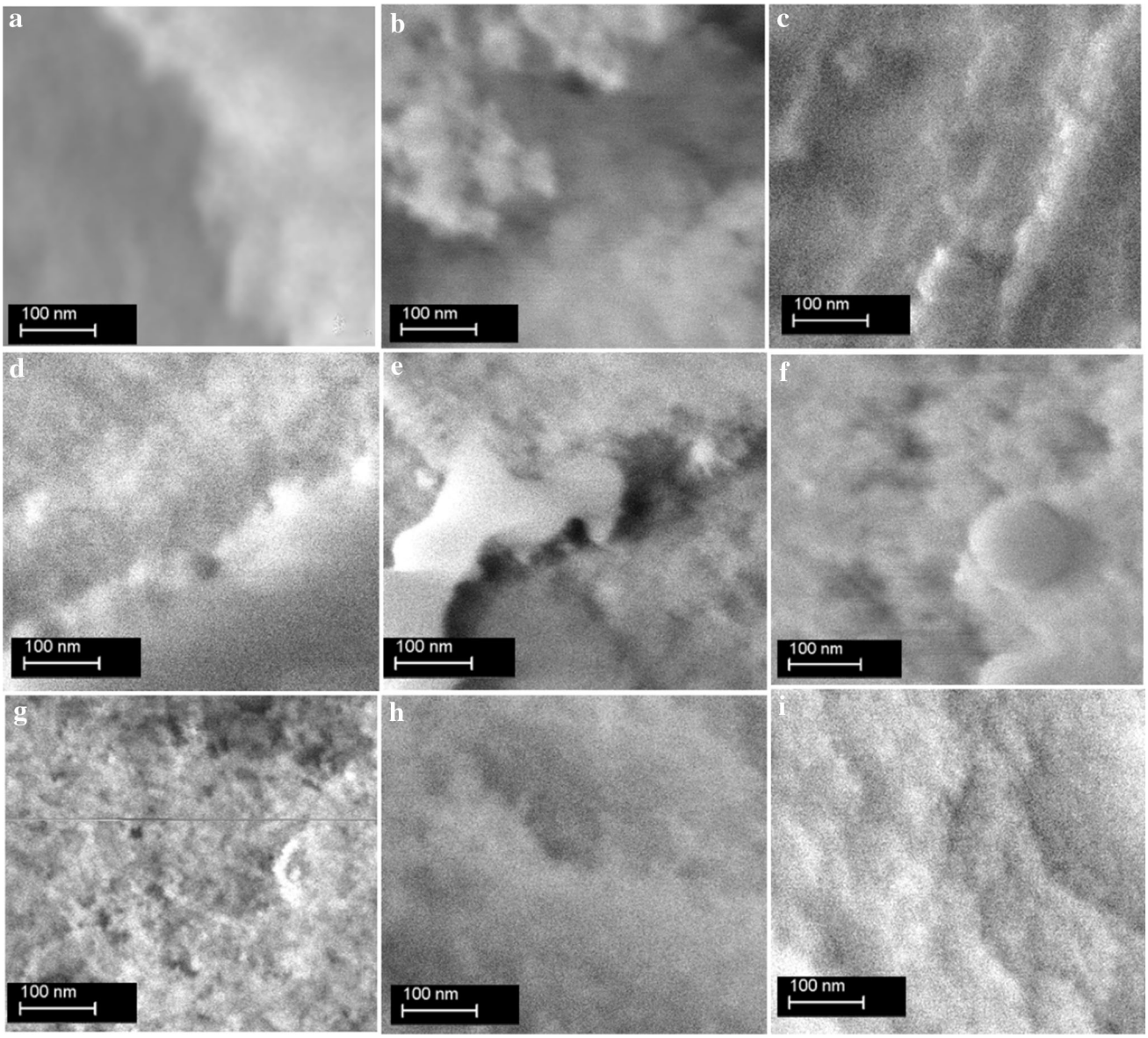

Fig. 6 SEM images of the surface morphology of the tested aerogels are shown for the following pH values: **a** 1, **b** 2, **c** 3, **d** 4, **e** 5, **f** 6, **g** 7, **h** 8, and **i** 9

Figure 8 shows the optical transmittance over discrete 100 nm bandwidth sections the visible spectrum normalized with respect to the total transmittance of each sample. Since the absorption coefficient of light by silica in the visible region is small, scattering should be the primary mode of attenuation [26]. When the inhomogeneities of the aerogel network are much smaller than visible wavelengths, nearly, isotropic scattering (Rayleigh scattering) is expected.

This scale of nanostructural feature corresponds to the M3 microstructure identified in "Morphology". The presence of nanostructural elements that are on the order of the visible spectrum, such as those found in the M1 microstructure, can cause Mie scattering. The fractal structures of the aerogel have been shown to scatter significantly by Alexander [27]. The maximum of this scattering was shown to occur when the wavelength is close to the size of the fraction. The M2 microstructure from Fig. 6 typifies this fractal microstructure and is observed in the pH = 7 and pH = 10 samples.

In Fig. 8, we also observe that the dispersion of scattering is relatively large for the M1 microstructure. This M1 morphology experiences strong scattering at the lower end of the visible spectrum that decreases with increasing wavelength. This scattering behavior is most likely due to strong interactions with its microstructural features in the

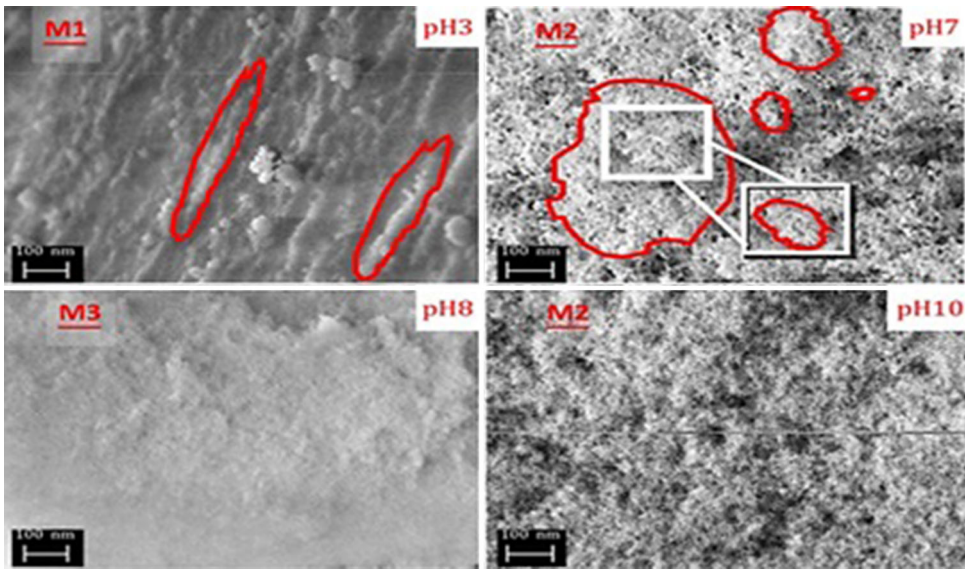

Fig. 7 SEM images for aerogel samples prepared with solutions of pH = 3, 7, 8, and 10. A range of fractal sizes from several tens to several hundred manometers can be seen in the pH = 7 sample (outlined in *red*) with a similar range of fractals exhibited by the pH = 10 sample. In contrast, samples starting from pH = 3 and 8 appear to be devoid of fractal structures over this size range

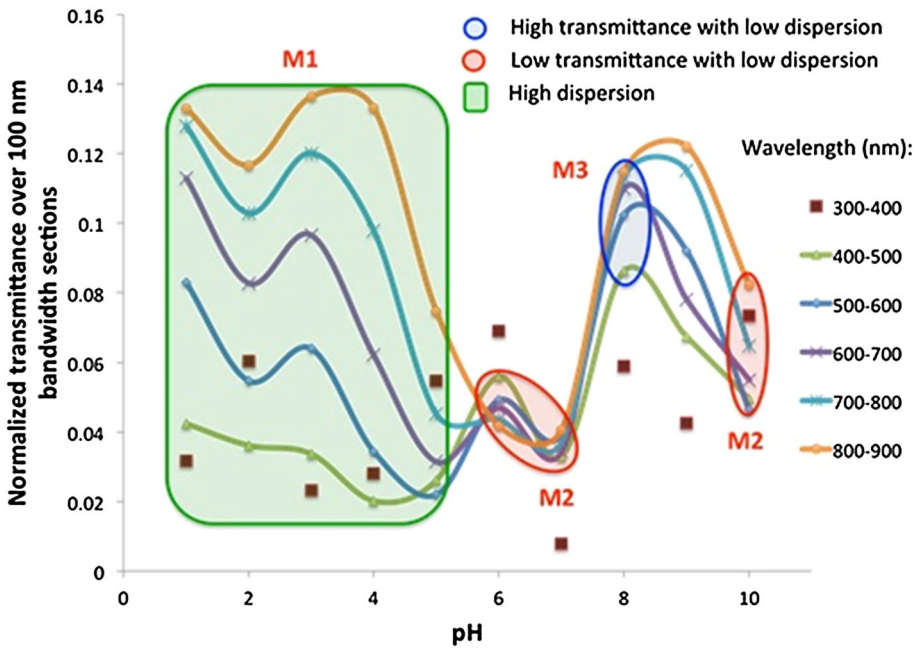

Fig. 8 Optical transmittance in 100 nm bandwidth segments over the visible spectrum. The transmittance values for the samples at each pH value are normalized by the total transmittance for that pH

sub-micrometer range with the majority of features lying in the 300–500 nm size range.

Thus, the M1 microstructure results in moderate overall transmission but high dispersion. The fractal morphology, M2, scatters nearly equally well over the whole visible spectral range due to the hierarchically repeated features that span the visible range. This results in low transmission and low dispersion. The isotropic structure scatters very poorly over the whole visible range, resulting in high transmission and low dispersion.

As stated earlier, excluding final pH values, all aerogel samples were prepared under the same conditions, reaction temperature, molar ratio of TEOS and water, and aging time, so the pH of the reaction solution is the primary influence on the microstructure and the resulting optical properties [28]. While an acid-catalysed reaction demands high electron density, a base-catalysed reaction demands low electron density, and therefore, the condensation process will result in more linear features under an acidic environment and a more branched network under a basic environment [13].

In addition, all samples are made solely of silica; therefore, the aerogel network structure is the individual factor that gives rise to any variation in the transmittance (Fig. 1). The difference in refractive index between silica network and the pore material (air in the case of aerogel) may be a reasonable source of light scattering, as the pores may act as scatter centres.

In general, as the acidity of the sol decreases, transmittance will decrease as well, reaching a minimum value at pH = 7. Because the lowest reaction rate for hydrolysis occurs at pH = 7 [29], a lot of silica networks are still unreacted, so the electrophilic tendency of condensation terminates, and the alcohol condensation mechanism becomes favourable [30, 31]. This condition gives rise to more locally branched networks, leading to narrow pore sizes and small pore volumes, thus giving rise to dense network and then low transparency. The above mechanism may be reflected in the reduction in pore volume from the single-point method with respect to pH (Table 1). This relationship did not hold up for the aerogels synthesized under the basic conditions as the transmission increased significantly from pH = 7 to 8 (Fig. 2). The suggested relationship between pore volume and transparency is still valid as the pH value increases beyond 8 (Table 1; Fig. 2).

With regard to the odd behaviour in the case of pH = 2 sample, this pH value corresponds to the zero charge point of silica [13]. At this point, the condensation mechanism of silica changes from electrophilic to electrophobic, so the reduction in transmission here may be attributed to the same reasons as those for pH = 7 but to a lesser extent.

The IUPAC classification of hysteresis loops can help in the analysis of the liner isotherm plots, as presented in Fig. 3 [23]. The plots for the pH = 1, 2, 3, and 5 samples in Fig. 3a may be classified as H3, which is related to non-rigid aggregates of plate-like particles (slit-shaped pores). The plots for the pH = 6 and 7 samples (Fig. 3a) may be classified as H4, which is related to narrow slit pores, including pores in the microporous region. The plots belonging to the pH = 4, 8, 9, and 10 samples (Fig. 3b) can be classified as H1, which is related to well-defined cylindrical pore channels [23].

Except in the case of the pH = 4 sample, the mechanism that produced the linear isotherm plot can be divided into two branches: acidic and basic behaviour. This may be explained by the fact that silica has its isoelectrical point (IEP), the point at which the zeta potential is equal to zero, at approximately pH = 4, or 4.5, to be exact. At the IEP, the reaction rate for condensation is at a minimum; hence, the water condensation mechanism becomes favourable to the alcohol condensation mechanism [30]. This condition may give rise to less branchy networks and lead to large pore sizes, resulting in higher adsorption quantities at higher relative pressures.

The starting pH, therefore, strongly influences the resulting microstructure, and allows for the control of microstructure-dictated properties. The optical transmittance and dispersion can be tuned through pH control, with pH = 1–5 giving high dispersion, pH = 6–7 resulting in low transmittance and low dispersion, pH = 8 showing the best transmittance with the lowest dispersion, pH = 9 exhibiting high dispersion, and pH = 10 leading back to low transmittance and low dispersion.

Conclusions

We demonstrate a systematic correlation between the starting pH of the reactant mixture and the resulting microstructure then optical properties of silica aerogels. Specifically, the total transmittance over the visible range as well its dispersion is strongly governed by the effect that the starting pH has on their final microstructure. We categorize the observed microstructure into three main types: monostructural, which exhibits a repetition of elongated microstructural features several hundred nanometres in size based on its scattering behaviour; fractal, which shows a hierarchical repetition of structural features; and isotropic, which has no directionality to its microstructural features. The samples with a starting pH = 1–5 show high dispersion, those from pH = 6–7 show low transmittance and low dispersion, and the pH = 8 based on aerogel exhibits a combination of the best transmittance with the lowest dispersion. For a pH greater than 8, there is a transition to low transmittance and low dispersion. The optical transmittance and dispersion of synthesized silica aerogels can, therefore, be tuned through the single synthesis parameter of the reactant pH.

Acknowledgements We would like to acknowledge the National Science Foundation Nanostructured Materials for Energy Storage and Conversion (NESAC) IGERT program for traineeship support under Award Number 1069138.

References

1. Kistler, S.S.: Coherent expanded aerogels and jellies. Nature **127**, 741 (1931)
2. Schaefer, D.W., Keefer, K.D.: Fractal geometry of silica condensation polymers. Phys. Rev. Lett. **53**, 1383–1386 (1984)
3. Schaefer, D.W., Keefer, K.D.: Structure of random porous materials: silica aerogel. Phys. Rev. Lett. **56**, 2199–2202 (1986)

4. Roldugin, V.I.: The characteristics of fractal disperse systems. Russ. Chem. Rev. **72**, 913–937 (2003)
5. Roldugin, V.I.: Self-organization of nanoparticles at interfaces. Russ. Chem. Rev. **73**, 123–156 (2004)
6. Julien, R.: Fractal systems. Usp. Fiz. Nuak **157**, 339–357 (1989)
7. Fang, Y., Roy, R., Agrawal, D.K., Roy, D.M.: Transparent mullite ceramics from diphasic aerogels by microwave and conventional processings. Mat. Lett. **28**, 11–15 (1996)
8. Gurav, J.L., Jung, I.K., Park, H.H., Kang, E.S., Nadargi, D.Y.: Silica aerogel: synthesis and applications. J. Nanomat. **2010**, 1–11 (2010)
9. Smirnova, I., Suttiruengwong, S., Arlt, W.: Feasibility study of hydrophilic and hydrophobic silica aerogels as drug delivery systems. JNCS **350**, 54–60 (2004)
10. Fricke, J., Emmerling, A.: Aerogels preparation, properties, applications. In: Reisfeld, R., Jørgensen, C.K. (eds.) Chemistry, Spectroscopy and Applications of Sol-Gel Glasses. Springer, Berlin (1992)
11. Aegerter, M.A., Leventis, N., Koebel, M.M.: Aerogels Handbook: Advances in Sol-Gel Derived Materials and Technologies. Springer Science + Business Media, New York (2011)
12. Schubert, U., Hüsing, N.: Synthesis of Inorganic Materials. Wiley-VCH, Weinheim (2004)
13. Iler, R.K.: The Chemistry of Silica: Solubility, Polymerization, Colloid and Surface Properties and Biochemistry of Silica, Chap 5, p. 209. Wiley, New York (1979)
14. Lee, S., Cha, Y.C., Hwang, H.J., Moon, J.W., Han, I.S.: The effect of pH on the physicochemical properties of silica aerogels prepared by an ambient pressure drying method. Mater. Lett. **61**, 3130–3133 (2007)
15. Kickelbick, G.: Hybrid Materials: Synthesis, Characterization and Applications, 1st edn. Wiley-VCH Verlag, Weinheim (2007)
16. Sukul, D., Sen, S., Dutta, P., Bhattacharyya, K.: Isomerization and fluorescence depolarization of merocyanine 540 in polyacrylic acid effect of pH. Proc. Indian Acad. Sci. (Chem. Sci.) **114**, 501–511 (2002)
17. Gentilini, S., Ghajeri, F., Ghofraniha, N., Di Falco, A., Conti, C.: Optical shock waves in silica aerogel. Opt. Express **22**, 1667–1672 (2014)
18. Emmerling, A., Petricevic, R., Beck, A., Wang, P., Scheller, H., Fricke, J.: Relationship between optical transparency and nanostructural features of silica aerogels. JNCS **185**, 240 (1995)
19. Zhao, L., Sungwoo, Y., Bhatia, B., Strobach, E., Wang, E.N.: Modeling silica aerogel optical performance by determining its radiative properties. AIP Adv. **6**, 025123 (2016)
20. Buratti, C., Moretti, E., Zinzi, M.: High energy-efficient windows with silica aerogel for building refurbishment: experimental characterization and preliminary simulations in different climate conditions. Buildings **7**, 8 (2017)
21. Kanamori, K., Aizawa, M., Nakanishi, K., Hanada, T.: New transparent methylsilsesquioxane aerogels and xerogels with improved mechanical properties. Adv. Mater. **19**, 1589 (2007)
22. Budunoglu, H., Yildirim, A., Guler, M.O., Bayindir, M.: Highly transparent, flexible, and thermally stable superhydrophobic ORMOSIL aerogel thin films. ACS Appl. Mater. Interfaces. **3**, 539 (2011)
23. Sing, K.S.W., Everett, D.H., Haul, R.A.W., Moscou, L., Pierotti, R.A., Rouquerol, J., Siemieniewska, T.: Reporting physisorption data for gas/solid systems with special reference to the determination of surface area and porosity (recommendations 1984). Pure Appl. Chem. **57**, 603–619 (1985)
24. Emmerling, A., Petricevic, R., Beck, A., Wang, P., Scheller, H., Fricke, J.: Relationship between optical transparency and nanostructural features of silica aerogels. JNCS **185**, 240–248 (1995)
25. Tillotson, T.M., Hrubesh, L.W.: Transparent ultralow-density silica aerogels prepared by a two-step sol-gel process. JNCS **145**, 44–50 (1992)
26. Athmuri, K., Marinov, V.R.: Optically transparent and structurally sound silica aerogels: insights from a process study. Adv. Mater. Sci **12**, 5–16 (2012)
27. Alexander, S.: Vibrations of fractals and scattering of light from aerogels. Phys. Rev. B **40**, 7953–7965 (1989)
28. Lee, J.H., Choi, S.Y., Kim, C.E., Kim, G.D.: The effects of initial sol parameters on the microstructure and optical transparency of TiO_2–SiO_2 binary aerogels. J. Mater. Sci. **32**, 3577–3585 (1997)
29. Sinkó, K.: Influence of chemical conditions on the nanoporous structure of silicate aerogels. Mater. **3**, 704–740 (2010)
30. Brinker, C.J., Sehgal, R., Hietala, S.L., Deshpande, R., Smith, D.M., Loy, D., Ashley, C.S.: Sol-gel strategies for controlled porosity inorganic materials. J. Membr. Sci. **94**, 85–102 (1994)
31. Brinker, C.J., Sherer, G.W.: Sol-Gel Science; The Physics and Chemistry of Sol-Gel Processing, 1st edn. Academic Press Inc, San Diego (1990)